Downloaded from orbit.dtu.dk on: Aug 26, 2019

DTU Library

A method to correct coordinate distortion in EBSD maps

Zhang, Yubin; Elbrønd, Andreas Benjamin; Lin, Fengxiang

Published in:
Materials Characterization

Link to article, DOI:
10.1016/j.matchar.2014.08.003

Publication date:
2014

Link back to DTU Orbit

Citation (APA):
Zhang, Y., Elbrønd, A. B., & Lin, F. (2014). A method to correct coordinate distortion in EBSD maps. Materials Characterization, 96, 158-165. https://doi.org/10.1016/j.matchar.2014.08.003

General rights
Copyright and moral rights for the publications made accessible in the public portal are retained by the authors and/or other copyright owners and it is a condition of accessing publications that users recognise and abide by the legal requirements associated with these rights.

- Users may download and print one copy of any publication from the public portal for the purpose of private study or research.
- You may not further distribute the material or use it for any profit-making activity or commercial gain
- You may freely distribute the URL identifying the publication in the public portal

If you believe that this document breaches copyright please contact us providing details, and we will remove access to the work immediately and investigate your claim.

A method to correct coordinate distortion in EBSD maps

Y.B. Zhang *, A. Elbrønd, F.X. Lin

Danish-Chinese Center for Nanometals, Section for Materials Science and Advanced Characterization, Department of Wind Energy, Technical University of Denmark, Risø campus, DK-4000 Roskilde, Denmark

Abstract: Drift during electron backscatter diffraction mapping leads to coordinate distortions in resulting orientation maps, which affects, in some cases significantly, the accuracy of analysis. A method, thin plate spline, is introduced and tested to correct such coordinate distortions in the maps after the electron backscatter diffraction measurements. The accuracy of the correction as well as theoretical and practical aspects of using the thin plate spline method is discussed in detail. By comparing with other correction methods, it is shown that the thin plate spline method is most efficient to correct different local distortions in the electron backscatter diffraction maps.

Key words: Electron backscatter diffraction (EBSD), thin plate spline (TPS), electron channelling contrast (ECC), transmission electron microscopy (TEM), recrystallization

1. Introduction

Electron backscatter diffraction (EBSD) in a scanning electron microscope (SEM) has been widely used to characterize microstructure due to the wide availability of SEMs, the ease of sample preparation from bulk, the user friendly software for data collection and analysis, and the high speed of data collection [1-3]. With EBSD, individual grain orientations, local texture, and point-to-point

orientation relationships can be determined routinely on the surfaces of bulk samples. In the last decade this technique has frequently been used for in-situ and ex-situ studies, from which dynamic information of microstructural evolution during thermal-mechanical processing has been reported [4-10].

Prior to EBSD measurements, regions of interest are defined, and grids, typically rectangles, covering the regions are specified. During scanning, thermal and mechanical drift of the electron beam and/or the sample (for instance mechanical instability of the column or the sample support, thermal expansion and contraction of the microscope components, and mechanical disturbances) can, however, distort the defined grid. Three examples of distortion are illustrated in Fig. 1, where the darker contaminated regions after EBSD measurements represent the real shapes of the scanned areas, which are clearly distorted to a different extent than the predefined rectangles. These distortions imply that the recorded coordinates of the EBSD maps do not correspond with the actual physical coordinates on the sample surface as predefined.

The drift is normally unpredictable and not constant, and it is more significant in the first few hours after the sample is mounted in the microscope and the electron beam is turned on, but less significant and relatively uniform afterwards (see Fig. 1 and Table 1). For EBSD scans lasting a few hours, the drift can result in coordinate differences from a few microns to dozens of microns along the x and/or y axes (see for example Fig. 1 and Table 1). Therefore, if large EBSD maps are collected using step sizes of several hundreds of nanometers or larger, conventional statistical information obtained from these maps, such as average boundary spacing, average grain size, and texture, can still be reliable because the drift-induced coordinate distortion is much smaller than the map sizes. However, if small electron beam step sizes such as 20-30nm, or even 2-5nm used in the transmission mode (i.e. the so-called t-EBSD or TKD (transmission Kikuchi diffraction) [11-13]) are utilized, the drift-induced coordinate

distortion can significantly affect the data because the drift speed is comparable to the step sizes (see Table 1). This problem has been widely recognized, and is solved generally either by cutting off the initial part of the EBSD map, thus excluding the most distorted part from the analysis, or by starting EBSD measurements when there is no significant drift, i.e. after a long waiting period. Some commercial EBSD packages allow drift correction during data acquisition using linear image correlation of forescatter images. However, the drift correction based on the image correlation alone cannot correct both the beam drift and the sample drift simultaneously. If the drift correction is not perfect, resulting EBSD maps can contain additional artifacts typically in the form of extended straight boundaries.

The drift problems become more critical when EBSD techniques are used together with other techniques, such as electron channeling contrast (ECC) and transmission electron microscopy (TEM), to characterize the same microstructures [14-17]. Due to the different imaging principles and acquisition time, the same microstructure characterized by EBSD can easily be more distorted than that with ECC/TEM. Consequently, quantitative comparison of some spatial-related microstructural parameters, such as grain shape and size, between the EBSD map and the ECC/TEM image can be difficult and not reliable.

Even more frequently, an EBSD map has to be compared with other EBSD maps of the same series collected during in-situ and ex-situ experiments [18-23]. In these cases, the coordinates in each of the EBSD map can be distorted relatively to the others because non-constant drift typically leads to different distortion among the series. For ex-situ EBSD experiments, unavoidable sample misalignment after the sample has been removed from the microscope for processing and remounted in the microscope even further worsens the coordinate distortion. Direct quantitative comparison among the

sequential EBSD maps, for example to measure local boundary migration distance during annealing [17], is rather difficult because of the distortion. As a result, although many in-situ and ex-situ studies have been conducted in the last decade, in most cases only qualitative analysis has been reported [18,21-23].

To the knowledge of the authors, no commercial software is available yet to correct the coordinate distortion in the EBSD maps after data acquisition. The aim of the present study is to propose a method to correct the coordinate distortion between true coordinates and recorded coordinates in the EBSD maps after the measurements have been completed. A method called the thin plate spline (TPS) method is chosen for the correction because it is a widely used and powerful method in image processing for correction of nonlinear distortion, such as that shown in Fig. 1. The theory of the TPS method and the correction process are briefly introduced in the next section. Then the method is used to correct an EBSD map in the section 3, and details related to the use of the TPS method are discussed in section 4.

2. Correction Method

In order to correct for the distortion of the recorded coordinates in an EBSD map, a reference distortion-free image, e.g. an electron channelling contrast (ECC) image (see the section 4.1), that has the same or overlapping contents is assumed to be available. Image registration [24] is then conducted to find a computational way to determine the point-by-point (pixel-by-pixel) correspondence between the EBSD map and the reference image. The image registration is generally carried out in two steps [24]. First, a number of control points (CPs) are selected from the reference image and the EBSD map, and correspondence is established between them. Second, the positions of corresponding CPs in the images are used to determine a transformation function that is in turn used to map the rest of the points

in the images. In the present study the CPs are selected manually and their correspondence is automatically established. They are denoted as (x_i, y_i) and (X_i, Y_i) (i = 1, 2, 3, …, n) in the reference image and EBSD map, respectively.

For the second step, many transformation functions can be used. Well-known examples are rotation, translation, similarity, affine, and perspective transformations, which transform images rigidly, i.e. line features in the image are reserved after transformation [24]. The coordinate distortion in the EBSD map is, however, generally nonlinear (see Figs. 1a and 1b), and nonrigid transformation functions are needed. In nonrigid image registration, thin plate spline (TPS) is a widely used transformation function [24], for example, in the registration of remote sensing images [25] and in the registration of medical images [26]. The TPS is a 2D generalization of the cubic spline, and in its regularized form it includes the affine transformation as a special case [26].

The TPS generally has the following form:

$$f(x,y) = a_1 + a_x x + a_y y + \sum_{i=1}^{n} w_i U(|(x_i, y_i) - (x,y)|) \quad (1)$$

where the kernel function U(r) is defined as

$$U(r) = r^2 \log r^2 \quad (2)$$

and $U(0) = 0$. The first three terms in Eq. 1 correspond to the linear part that defines a flat plane that best matches all the CPs, i.e. the affine part. The last term corresponds to the bending forces provided by n CPs with w_i varying for each CP. The unknown coefficients of w_i, a_1, a_x, a_y are solved based on the coordinates of the two sets of corresponding CPs, (x_i, y_i) and (X_i, Y_i). Details on calculation procedure are presented in the Appendix.

By substituting the calculated values of w_i, a_1, a_x, a_y in Eq. 1, and scanning the reference image, the pixel to pixel relation from each pixel (x, y) in the reference image to its corresponding pixel (X, Y) = $f(x, y)$ in the original EBSD map can be determined, hence the corrected EBSD map can be reconstructed. However, the resolution of the corrected EBSD map after reconstruction is changed to that of the reference image. To preserve the resolution of the original EBSD map, in practice the CP coordinates in the reference image are divided by a factor that is a ratio of the resolution of the original EBSD map to that of the reference image. This procedure is equivalent to resizing the reference image to the same resolution of the original EBSD map. In this way, new values for the coefficients of w_i, a_1, a_x, a_y, and hence new pixel to pixel relation between the resized reference image and the original EBSD map are obtained. The corrected EBSD map, which matches the resized reference image and has the same resolution of the original EBSD map, is then reconstructed pixel-by-pixel by copying EBSD data (including, for example, Euler angles, band contrast (BC), MAD value) from the original EBSD map according to the new pixel to pixel relation.

3. Example application of the method

3.1. Experimental

A partially recrystallized pure nickel sample was used to test the correction method. The sample was annealed at 320°C for 5 min after cold rolling to 96% reduction in thickness [20]. After mechanical polishing with 1 μm grit diamond suspension and chemical polishing with Struers OP-S suspension, EBSD measurements were conducted in a Zeiss Supra-35 thermal field emission gun SEM using HKL Channel 5 system. An area of 120 × 120 μm^2 was scanned with a step size of 200 nm on a longitudinal section (defined by the normal direction (ND) and rolling direction (RD)) of the sample. The EBSD

measurements were conducted with the electron beam scanning within a predefined square grid of 600 × 600 vertically from left to right, and it took ~5h in total. The actually mapped region is seen as the darker region in Fig. 1b. The same area was characterized using the electron channelling contrast (ECC) techniques in the same SEM. The ECC image was taken at zero tilt within 8 min. It has a spatial resolution of 92.5 nm/pixel, and is used as the reference image for the correction.

The ECC image and the EBSD map showing the partially recrystallized microstructure are given in Figs. 2a and 2b, respectively. Based on the ECC image and EBSD map, control points (CPs) were selected manually at recrystallizing grain boundaries and triple junctions between recrystallized grains. To investigate effects of the number of CPs and of their spatial distribution, 36, 54, and 60 pairs of CPs were utilized, and their coordinates are plotted in Fig. 2c-e. The 36 CP pairs in Fig. 2c were selected to be relatively uniformly distributed over the EBSD map. Fig. 2d contains also these 36 pairs and additional 18 pairs in the left 1/4 part of the EBSD map. Fig. 2e contains 6 additional pairs in the right 3/4 part of the EBSD map.

3.2. Correction results

With the CP pairs in Fig. 2c-e, the EBSD map was corrected using the TPS method, which was implemented using Matlab code[1]. To evaluate the correction results, two independent comparisons were carried out. Firstly, the curved outlines of the corrected EBSD band contrast (BC) maps in Fig. 3 were compared to that of the real scanned area in Fig. 1b, to get a fist impression of the efficiency of the correction method. This is an important validation as the shaded image is not at all used in the correction procedure. The angle marked in Fig. 1b describe the observed drift extent for the first ~50

[1] The program package can be downloaded from www.nanometals.dk

line scans of the EBSD map, and the distances, d_y, represents the maximum drift distance along the y axis. As summarized in Table 2, these values can directly be compared to those measured from Fig. 3. Taking the measurement error of ~200nm and 1° for the measured d_y and angles, respectively, into account, the large differences in the measured distances for the left 1/5 part of the map between Fig. 1b and Fig. 3a evidently imply that the 36 pairs of CPs do not correct the overall shape of the left 1/5 part of the map well (see Table 2). In contrast, the small differences of 400nm in the measured distances for the right 4/5 part of the map between Fig. 1b and Fig. 3a are close to the error of measurements (~200nm), suggesting a good correction for this part. Similarly, comparisons of the distances and angles between Fig. 1b and Fig. 3b as well as 3c suggest that both the 54 and 60 pairs of CPs correct the overall shapes of the whole maps well.

A more detailed evaluation of the correction results is further conducted by comparing the local microstructures in the corrected EBSD maps with the ECC image in Fig. 2a. For example, focusing on the boundary marked by the white arrow in Fig. 2a, the boundary is still aligned at ~20° to the horizontal direction in Fig. 3a, indicating a less satisfactory correction for this left part of Fig. 3a, whereas the same boundary becomes horizontally aligned in Fig. 3b and c, after the extra 18 pairs of CPs are added to this part of the map. To illustrate the detailed comparison, the local microstructures within the two rectangles in Fig. 3 are enlarged and shown in Fig. 4. The two regions are selected to be representative for the left 1/5 and right 4/5 parts of the map. By comparing these BC maps (Fig. 4a-c) with the ECC images from exactly the same regions (see Fig. 4d), it is evident that a very good correction is obtained for the region from the right 4/5 part in Fig. 4a, and for both regions in Fig. 4b and 4c. The EBSD subsets shown in Fig. 4b are further superimposed on the ECC subsets to evaluate the correction accuracy (see Fig. 4e). For visualization, the EBSD subsets are colored and cut to be

smaller than the ECC subsets. Note also that the ECC subsets in Fig. 4e are resized by a factor of 200nm/92.5nm = 2.16 to the same resolution of the EBSD map (This number are given by the step size of the EBSD map and the resolution of the ECC image). By comparing the positions of all the recrystallization boundaries at the interfaces between the EBSD subsets and ECC subsets, it is evident that a satisfactory match with either no shift or 1 pixel shift between the corrected EBSD map and the resized ECC image is achieved based on the 54 pairs of CPs.

The difference between two corrected images in Fig. 3 has also been analyzed and shown in Fig. 5, where the first image (purple) is overlaid on the second image (green). Areas that have same orientations appear in grey, while different oriented areas appear in purple or green. As expected, large difference is found in the left 1/5-1/4 part of the map in Fig. 5a. Not much difference is seen for the rest of the map, suggesting that the extra 18 pairs of CPs affect mainly local area around them, but do not have much effect away from them. In contrast, in Fig. 5b much smaller local shift of ~1 pixel is seen.

4. Discussion

4.1. Reference images

One may consider many ways of obtaining a proper distortion-free reference image. Although images obtained from optical microscope are distortion-free, they are not suitable as reference images because of the low spatial resolution, 0.25-1 μm/pixel. And more importantly, the condition of sample surfaces for optical imaging is generally different from that for EBSD mapping. A sample subjected to optical imaging has to be polished again before EBSD measurements, and vice versa, which means the optical image and the EBSD map are not taken from the same sample surface.

In the present study, an ECC image is used as the reference image. Use of ECC images as reference images has the following four major advantages. i) ECC techniques are orientation sensitive, which allows identification of microstructural features and easy selection of CPs; ii) ECC images can be taken from the same sample surface after EBSD measurements without any additional surface treatment needed; iii) The spatial resolution of ECC images can easily be higher than that of EBSD maps, which is beneficial to achieve a high precision of CP positions (see the section 4.3 below); iv) Since ECC images are taken at 0° tilt angle and within a short acquisition time (typically a few minutes), drift is almost constant and small, and can thus be ignored. Thanks to these advantages, ECC images are for most cases the first choice of reference images to correct EBSD maps.

TEM images can also be used as reference images. Similar to ECC techniques, TEM is orientation sensitive, and has normally a very high spatial resolution. The surface condition for TEM samples are in most cases suitable for direct EBSD measurements [14-16]. Since the acquisition time for TEM images is in the order of seconds, the spatial distortion in the images caused by beam drift is very small. Besides, the recently developed t-EBSD (or TKD) techniques [11-13] allows orientation mapping on TEM foils in the transmission mode, which provides more possibilities in using EBSD in combination with TEM. As the t-EBSD techniques are most suitable for nanostructured materials, it is expected that TEM images of nanostructures may be used as reference images in the future.

Once an EBSD map has been corrected using another reference image, the corrected EBSD map can also be used as the reference image to correct other EBSD maps of a same series that is obtained in situ or ex situ at the same surface area, or even after serial sectioning [27-29]. Finally, if only the differences between two EBSD maps are of interest, the second EBSD map may directly be corrected

with reference to the first EBSD map, i.e. the first image may be used as a reference image even without correction.

4.2. Effects of number and distribution of control points

Figs. 3-5 show that the number and distribution of CPs directly affect the correction results. To obtain a satisfactory correction on both local and global scales, the CPs need to be distributed over the whole map because the TPS correction is sensitive to the local CPs (see Fig. 5). The number of CPs required for a good correction can be different from location to location depending on the local distortion extent, being higher at places where the distortion is more significant. For example in the present study, to enable a good correction for the less significant distortion in the 4/5 right part of the map, a relatively small CP number of ~0.8 per 100 × 100 pixel area is sufficient (Fig. 3). In contrast, for the left 1/5 part of the map where the drift speed on average is ~4 times of that for the rest part of the map (see Table 1), the number of CPs needs to be ~2.9 per 100 × 100 pixel area, which is ~4 times of that for the 4/5 right part of the map. Moreover, the total number of CPs needed to correct an EBSD map well is determined by the grid size of the map; the larger the grid size is, the more CPs are needed.

In general, for a given EBSD map the correction quality increases with increasing number of CPs. But considering the fact that selecting CPs is a time consuming process, it is not worth keeping increasing the number of CPs once satisfactory correction is obtained. In practice, Matlab provides a build-in function ‘cpselect’, allowing high magnification view of local microstructure as well as online selecting, storing and editing CPs, which significantly simplifies the selecting process. The map shown in Fig. 5 can be used to estimate whether a selected number of CPs is sufficient for a given EBSD map. After extra CPs are added, if no significant difference is observed around these extra CPs (see for example

Fig. 5b), a sufficient number of CPs for the area is reached; otherwise more CPs are needed. The CP selection is thus typically conducted through an iterative process. Different parts of the map, in particular regions with different distortion extent, need to be considered separately. Alternatively, a more precise way to estimate the correction results, the corrected EBSD map is compared directly to the reference image by matching the corrected EBSD map semitransparent and superimposing it on top of the reference image. A satisfactory correction is obtained when certain correction accuracy is archived (see the section 4.3).

4.3. Effect of noise on correction accuracy

During coordinate transformation, the TPS method transforms the CP coordinates in the EBSD map exactly to those in the reference image [26,30]. However, during CP pair selection, the CP positions in the EBSD map can be slightly deviated from those in the reference image because of noise in the EBSD map (e.g. non-indexed pixels) and in the reference image, i.e. uncertainty exists between correspondent CP pairs. This uncertainty will be directly inherited in the corrected EBSD map, reducing thereby the correction accuracy. Besides the noise, if the spatial resolution of the reference image is poorer than that of the EBSD map, the accuracy in finding the same features in the reference image as those in the EBSD map is reduced, and the correction accuracy is then limited by the resolution of the reference image.

In practice, it is advisable that the reference image is acquired with a higher spatial resolution than that of the original EBSD map to reduce the CP pairs' correspondence uncertainty. A low noise level (i.e. high indexed rate) of the original EBSD map is also beneficial to reducing the uncertainty level. CPs are better selected at places where features can easily be distinguished, such as at triple junctions of

recrystallized grains and at recrystallizing grain boundaries. In the present study, thanks to the high spatial resolution of the ECC image, the correction accuracy is determined by the resolution of the original EBSD map to be ~1 pixel, which is the accuracy of the CP positions.

4.4. Comparison with other methods

A method based on image entropy and mutual information, which is often used in data fusion, has previously been introduced into correction of EBSD maps [31]. However, in this previous study only linear transformation functions, such as affine transformation, were considered in the correction. EBSD maps similar to the one presented here, where distortion is complex and nonlinear, can evidently not be corrected well with solely affine transformation, and thus this method will not be considered for comparison.

Polynomials have also been used as transformation functions to correct nonlinear distortion in the EBSD maps collected during serial sectioning [32]. To compare with the TPS approach (Eq. 1), these functions were utilized to correct the present EBSD map (Fig. 2b). Figs. 6a and b show the corrected EBSD maps using polynomials of second order and fourth order, respectively. For both cases, the 54 pairs of CPs as shown in Fig. 2d are used. Simply by comparing the angles and distances, used to quantify the curved outlines of the corrected EBSD maps, in Fig. 6 with those in Fig. 1b, it is apparent that the correction with polynomials is less satisfactory, not to mention detailed comparison of local microstructure between the corrected EBSD maps and the ECC image in Fig. 2a (see for example the boundary marked by white arrows).

The less satisfactory correction using polynomials is partly because the curved outline of the distorted shapes is so complex that the related polynomial functions cannot fit it well. As a result, the polynomials transform corresponding CP coordinates only approximately to each other. Therefore even the CP coordinates in the corrected EBSD map do not match those in the reference image. As the order of polynomials increases from 2 to 4, the outline of the corrected map in Fig. 6b becomes more similar to that shown in Fig. 1b. At the same time, the difference (root-mean-squared (RMS) errors) between CP coordinates in the corrected EBSD map and in the reference images is reduced. Although by keeping increasing the order of polynomials, the RMS errors can be further reduced, polynomials of very high orders are usually not advisable because they can produce fluctuations away from the CPs and prediction of their behaviors from their coefficients is very difficult [30].

As a comparison, with the TPS method, the RMS errors between the CP coordinates in the corrected EBSD map and in the reference image is 0, as the TPS method transform corresponding CP coordinates exactly to each other [30]. Additionally, the TPS method is less affected by the overall shape of the distortion, because as long as a sufficient number of CPs is selected, different local distortions can be corrected well, and so does the overall shape of the distortion. For EBSD maps, such as the present one that contains locally varying distortions, the correction with the TPS method is therefore much more satisfactory than that with polynomials.

5. Conclusions

The thin plate spline (TPS) method is suggested for post-measurements correction of the coordinate distortion in EBSD maps, which is caused by drift of electron beam and/or sample during the EBSD measurements. The method is based on using a distortion-free image as a reference image, and on

manually selected control points (CPs) from the reference image and the EBSD map (to be corrected). It has been found that:

i) The TPS method is a sophisticated method to correct nonlinear distortion in the EBSD maps. Compared with other correction methods, such as using polynomials, the TPS method corrects more precisely EBSD maps that contain locally different extents of distortion.

ii) ECC and TEM images are good choices as reference images to correct EBSD maps because of their high resolution and negligible distortion. Once an EBSD map has been corrected using the TPS method, the corrected map can also be used as reference image to correct other EBSD maps in a series of dynamic measurements.

iii) A certain number of CPs distributed over the whole EBSD map is needed to enable a good correction using the TPS method. The number of CPs per unit area needs to be higher at places where local distortions are more severe than at places where local distortions are minor.

iv) The correction quality generally increases with increasing number of CPs, and an accuracy of ~1 pixel over the entire EBSD map can be achieved.

Acknowledgements

The authors gratefully acknowledge the support from the Danish National Research Foundation (Grant No DNRF86-5) and the National Natural Science Foundation of China (Grant No. 51261130091) to the Danish-Chinese Center for Nanometals, within which this work has been performed. Prof. Juul Jensen D., Prof. Godfrey A and Dr. Mishin O. are gratefully thanked for their valuable discussions and comments on the manuscript.

References

[1] Schwartz AJ, Kumar M, Adams BL, Field DP. Electron Backscatter Diffraction in Materials Science. 2ed ed. Springer 2009

[2] Humphreys FJ. Quantitative metallography by eletron backscattered diffraction. J Microsc 1999; 195:170-85.

[3] Lassen NCK, Juul Jensen D, Conradsen K. On the statistical analysis of orientation data. Acta Cryst. 1994;A50:741-748.

[4] Hurley PJ, Humphreys FJ. A study of recrystallization in single-phase aluminium using in-situ annealing in the scanning electron microscope. J Microscopy 2003; 213: 225-234.

[5] Kerisit C, Loge RE, Jacomet S, Llorca V, Bozzolo N. EBSD coupled to SEM in-situ annealing for assessing recrystallization and grain growth mechanisms in pure tantalum. J Microscopy 2013; 250: 189-99.

[6] Quey R, Piot D, Driver JH. Microtexture tracking in hot-deformed polycrystalline aluminium: Experimental results. Acta Mater 2010; 58: 1629-42.

[7] Lens A, Maurice C, Driver JH, Grain boundary mobilities during recrystallization of Al-Mn alloys as measured by in-situ annealing experiments. Mater Sci Eng A 2005; 403: 144-53.

[8] Allain-Bonasso N, Wagner F, Berbenni S, Field DP. A study of the heterogeneity of plastic deformation in IF steel by EBSD. Mater Sci Eng A 2012; 548: 52-63.

[9] Piazolo S, Jessell MW, Prior DJ, Bons PD, The integration of experimental in-situ EBSD observations and numerical simulations: a novel technique of microstructural process analysis. J Microscopy 2004; 213: 273-284.

[10] Tian H, Suo HL, Mishin OV, Zhang YB, Juul Jensen D, Grivel J-C. Annealing behavior of a nanostructured Cu-45at.%Ni alloy. J Mater Sci 2013; 48: 4183-90.

[11] Keller RR, Geiss RH, Transmission EBSD from 10nm domains in a scanning electron microscope. J Microscopy 2012; 245: 245-251.

[12] Trimby PW, Orientation mapping of nanostructured materials using transmission Kikuchi diffraction in the scanning electron microscope. Ultramicroscopy 2012; 120: 16-24.

[13] Brodusch N, Demers H, Gauvin R, Nanometres-resolution Kikuchi patterns from materials science specimens with transmission electron forward scatter diffraction in the scanning electron microscope. J Microscopy 2013;250:1-14.

[14] Suzuki S, Features of transmission EBSD and its application. JOM 2013;65:1254-63.

[15] Mishin OV, Godfrey A, Ostensson L, Comparative microstructural characterization of a friction-stir-welded aluminum alloy using TEM and SEM-based techniques. Metal. Mater. Trans. 2006; 37A:489-96.

[16] Godfrey A, Mishin O, Liu Q, Processing and interpretation of EBSD data gathered from plastically deformed metals. Mater. Sci. Tech. 2006;22:1263-70.

[17] Zhang YB, Godfrey A, Juul Jensen D, In-situ investigation of local boundary migration during recrystallization. Metal. Mater. Trans. A 2014; 45:2899-2905.

[18] Field DP, Bradford LT, Nowell MM, Lillo TM. The role of annealing twins during recrystallization of Cu. Acta Mater 2007; 55: 4233-41.

[19] Zhang YB, Godfrey A, Liu Q, Liu W, Investigation of boundary migration during grain growth in fully recrystallized high purity nickel. Mater Sci and Tech 2010; 26:197-202.

[20] Zhang YB, Godfrey A, Liu Q, Liu W, Juul Jensen D, Analysis of the growth of individual grains during recrystallization in pure nickel. Acta Mater 2009; 57: 2631-2639.

[21] Piazolo S, Bestman M, Prior DJ, Spiers CJ. Temparature dependent grain boundary migration in deformed-then-annealed material: Obsercations from experimentally deformed synthetic rocksalt. Tectonophysics 2006; 427: 55-71.

[22] Bestman M, Piazolo S, Spiers CJ, Prior DJ. Microstructure evolution during initial stages of static recovery and recrystallization: new insight from in-situ heating experiments combined with electron backscatter diffraction analysis. J Structural Geology 2005; 27: 447-57.

[23] Yu TB, Hansen N, Huang X, Recovery by triple junction motion in aluminium deformed to ultrahigh strains. Proc. Royal Society A 2011; 467: 3039-65.

[24] Goshtasby AA, Image registration, Principles, tools and methods. Springer-Verlag London Limited 2012.

[25] Goshtasby, A.: Registration of image with geometric distortion. IEEE Trans. Geosci. Remote Sens. 26(1), 60–64 (1988)

[26] Bookstein FL. Principal Warps: Thin-Plate Splines and the Decomposition of Deformations. IEEE Thans on Pattern Analysis and Machine Intelligence 1989; 6: 567-85.

[27] Fan GH, Zhang YB, Driver JH, Juul Jensen D, Oriented Growth during Recrystallization Revisited in Three Dimensions. Scr. Mater. 2014; 9-12.

[28] Zhang Y, Juul Jensen D, Zhang YB, Lin FX, Zhang Z, Liu Q. Three-dimentional investigation of recrystallization nucleation in a particle-containing Al alloy. Scr. Mater. 2012;67:320-323.

[29] Lin FX, Godfrey A, Juul Jensen D, Wither G. 3D EBSD characterization of deformation structures in commercial purity aluminum. Mater. Characterization. 2010;61:1203-10.

[30] Zagorchev L, Goshtasby A. A comparative study of transformation functions for nonrigid image registration. IEEE Trans. Image Proc. 2006;15:529-38.

[31] Gulsoy EB, Simmons JP, De Graef M, Application of joint histogram and mutual information to registration and data fusion problems in serial sectioning microstructure studies. Scr. Mater. 2009;60:381-384.

[32] Huang Y, Laflan B, Deal A, Spinelli I, Barbuto A, Hanlon T, Handling Misalignment and Drift in 3D EBSD Data Sets. Proceedings for 1st Internal Conference on 3D Material Science 2012; 165-170.

Appendix:

Solving coefficients for Eq. 1

Given the n pairs of CPs, (x_i, y_i) and (X_i, Y_i) (i = 1, 2, 3, …, n) in the reference image and EBSD map, respectively, this section provides a detailed procedure to calculate the coefficients, w_i, a_1, a_x, a_y in Eq. 1. The thin plate spline function $f(x, y)$ (Eq. 1) minimizes the bending energy

$$I_f = \iint_{\mathbf{R^2}} \left(\left(\frac{d^2 f(x,y)}{dx^2} \right)^2 + \left(\frac{d^2 f(x,y)}{dxdy} \right)^2 + \left(\frac{d^2 f(x,y)}{dy^2} \right)^2 \right) dxdy. \quad \text{A1)}$$

In order for $f(x, y)$ to have square integrable second derivatives, it is further required that

$$\sum_{i=1}^{n} w_i = 0, \quad \text{A2)}$$

and

$$\sum_{i=1}^{n} w_i x_i = \sum_{i=1}^{n} w_i y_i = 0, \quad \text{A3)}$$

Together with the conditions for the correspondent CPs, $f(x_i, y_i) = (X_i, Y_i) = v_i$, this yields a linear system for the TPS coefficients:

$$\begin{bmatrix} K & P \\ P^T & O \end{bmatrix} \begin{bmatrix} W \\ a \end{bmatrix} = \begin{bmatrix} V \\ o \end{bmatrix}, \quad \text{A4)}$$

where

$$K = \begin{bmatrix} 0 & U(r_{12}) & \dots & U(r_{1n}) \\ U(r_{21}) & 0 & \dots & U(r_{2n}) \\ \dots & \dots & \dots & \dots \\ U(r_{n1}) & U(r_{n2}) & \dots & 0 \end{bmatrix}, n \times n; \quad \text{A5)}$$

and

$$P = \begin{bmatrix} 1 & x_1 & y_1 \\ 1 & x_2 & y_2 \\ \dots & \dots & \dots \\ 1 & x_n & y_n \end{bmatrix}, 3 \times n; \quad \text{A6)}$$

and ^{T} is the matrix transpose operator, O is a 3×3 matrix of zeros, o is a 3×1 column vector of zeros, W and V are column vectors formed from w_i and v_i, respectively, a is the column vector with elements a_1, a_x, a_y.

Denote the $(n + 3) \times (n + 3)$ matrix in Eq. A4 by L, i.e.

$$L = \begin{bmatrix} K & P \\ P^T & O \end{bmatrix}, (n + 3) \times (n + 3), \quad \text{A7)}$$

and denote a column vector of length n + 3, $Y = (V \mid o)^T$, Eq. A4 can be expressed as

$$L^{-1}Y = (W \mid a)^T, \qquad \text{A8)}$$

Since all the left part of the equation are known, the unknown parameters w_i and a_1, a_x, a_y can be solved.

Figure and table captions:

Fig. 1 Examples of secondary electron images showing the carbon contaminated regions (darker shaded areas) after EBSD measurements on a longitudinal section of a partially recrystallized pure nickel sample. The electron beam scanned vertically from left to the right during EBSD mapping. The maximum drift distances along the y axis are marked in each image. The small rectangles marked by white arrows in (b) and (c) are caused by focusing. Detailed information about the EBSD measurements and drift speeds are summarized in Table 1. The dashed line in (b) separates the left 1/5 part of the scanned area from the rest 4/5 of the area. The angles and distances are used to quantify the curved outline of the maps, see text for details.

Fig. 2. Partially recrystallized microstructure of the pure nickel sample: (a) ECC image and (b) EBSD band contrast (BC) map. The EBSD map covers the region shown in Fig. 1b. The white arrow in (a) and (b) marks one boundary aligned almost parallel to ND in (a), but at ~35° to ND in (b), indicating a strong geometric distortion in the EBSD map. The microstructures within the two white rectangles in (a) are magnified in Fig. 4d. The contrast and brightness of the BC map are enhanced by 20% and 40%, respectively, to better see details of the map. (c), (d) and (e) show the coordinates of 36 pairs, 54 pairs and 60 pairs of CPs, respectively, selected from the ECC image (asterisk) and EBSD map (circles). The coordinates of the CPs in the ECC image were divided by 200/92.5 = 2.16 to the same scale of the EBSD map, and the shift of the average CP coordinates between ECC image and EBSD map was subtracted.

Fig. 3. Correction results for the EBSD BC maps that shown in Fig. 2b. Maps in (a)-(c) were corrected using CPs shown in Fig. 2(c)-(e), respectively. The white arrows mark the same boundary as the one marked in Fig. 2. The two white rectangles in (a)-(c) mark regions which are magnified in Fig. 4(a)-(c),

respectively. The contrast and brightness of the BC maps are enhanced by 20% and 40%, respectively, to better see details of the maps. The angles and distances are used to quantify the curved outline of the maps, see text for details.

Fig. 4. Enlarged view of the microstructures marked by the rectangles in Fig. 2a and Fig. 3: (a)-(c) EBSD BC maps from the areas framed in Fig. 3(a)-(c), respectively; (d) ECC images from the areas framed in Fig. 2a; (e) subsets of the EBSD map in (b) superimposed on the resized ECC subsets (resizing by a factor of 200nm/92.5nm = 2.16 to the same resolution of the EBSD map). For visualization, the EBSD subsets are shown in color and cut to be smaller than the ECC subsets in (e). Black pixels in the EBSD subsets in (e) are non-indexed.

Fig. 5. Maps showing the difference between two corrected maps in Fig. 3: (a) between corrections using the 36 and 54 pairs of CPs, and (b) between corrections using the 54 and 60 pairs of CPs. The maps were obtained by overlaying the first image (purple) on top of the second image (green). Areas with same orientations between two maps are shown in gray, while areas with different orientations are shown in green or purple. The microstructures marked by the rectangles are enlarged and shown as the inserts in both images.

Fig. 6. Correction results for the EBSD BC maps that shown in Fig. 2b using polynomials of second order (a) and fourth order (b), and using 54 CP pairs as shown in Fig. 3b. The angles and distances shown at the top are used are used to quantify the curved outline of the maps, see text for details. The white arrows mark the same boundary as the one shown in Fig. 2. The contrast and brightness of the BC maps are enhanced by 20% and 40%, respectively, to better see details of the map.

Table 1. Details for the three EBSD maps shown in Fig. 1. The electron beam step sizes used for all these three maps are 200 nm. The drift along the x direction is much smaller than that along the y direction, and is not listed in the table.

Table 2. Drift distances along the y direction, d_y, and angles measured for the upper curved outlines of corrected EBSD maps in Fig. 3 and of the real scanned area in Fig. 1b. The error in the measured distances in Fig. 1 is about 1 pixel that corresponds to ~200 nm, while the error in the measured angle is ~1°.

Table1

Table 1. Details for the three EBSD maps shown in Fig. 1. The electron beam step sizes used for all these three maps are 200 nm. The drift along the x direction is much smaller than that along the y direction, and is not listed in the table.

Scan No.	Grid size	Starting time* (h)	Scanned period (h)	Maximum deviation along y (μm)	Average drift speed along y (nm/s)
a	350 × 350	0.5	1.75	19.3	3
b	600 × 600	0.5	5	5.0/4.4**	1.4/0.3**
c	350 × 350	3	1.75	1.8	0.3

* Starting time means the time spent from turning the electron beam right after mounting the sample into the microscope until starting the EBSD scan.
** The two numbers are calculated for the left 1/5 part and the rest 4/5 part of the map as separated by the dashed line in Fig. 1b.

Table2

Table 2. Drift distances along the y direction, d_y, and angles measured for the upper curved outlines of corrected EBSD maps in Fig. 4 and of the real scanned area in Fig. 1b. The error in the measured distances in Fig. 1 is about 1 pixel that corresponds to ~200 nm, while the error in the measured angle is ~1°.

	Fig. 1b	Fig. 4a(36 CPs)	Fig. 4b(54 CPs)	Fig. 4c(60 CPs)
d_y for the left 1/5 part (μm)	5.0	3.4	4.6	4.6
d_y for the right 4/5 part (μm)	4.4	4.0	4.0	4.0
angle (°)	21	12	20	20

Figure1

Click here to download high resolution image

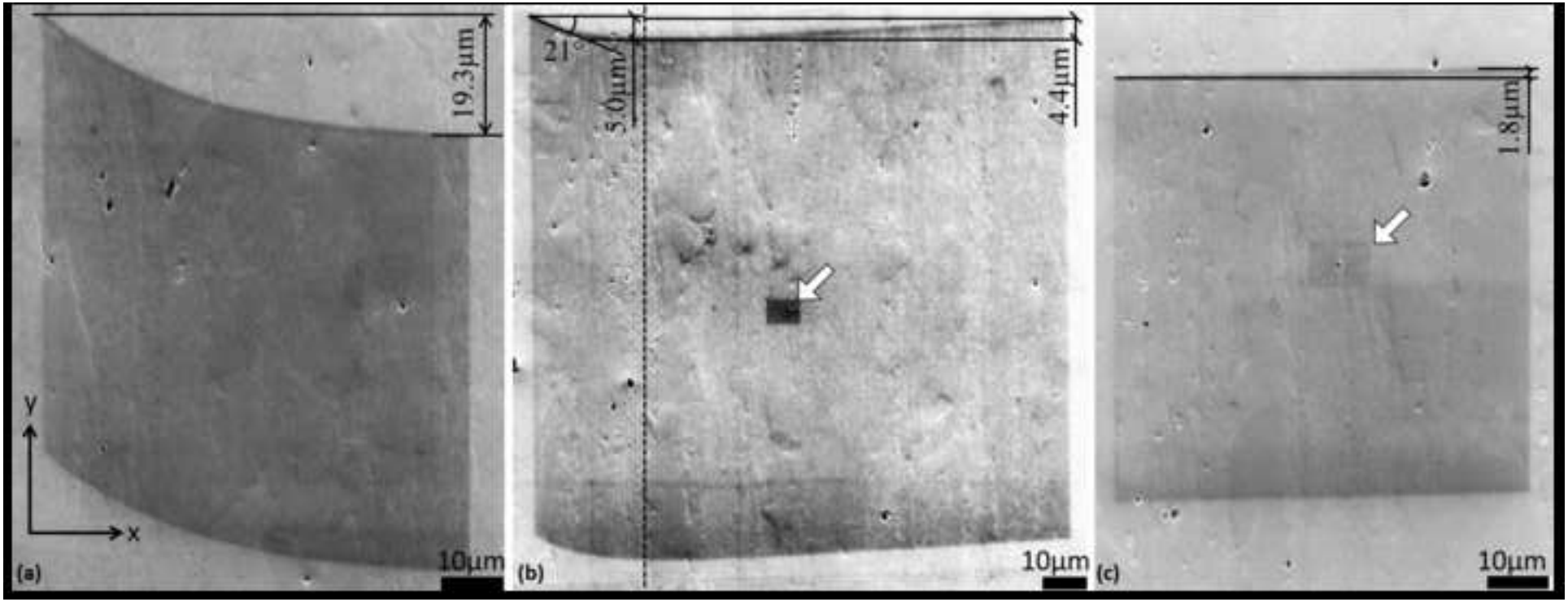

Figure2ab

Click here to download high resolution image

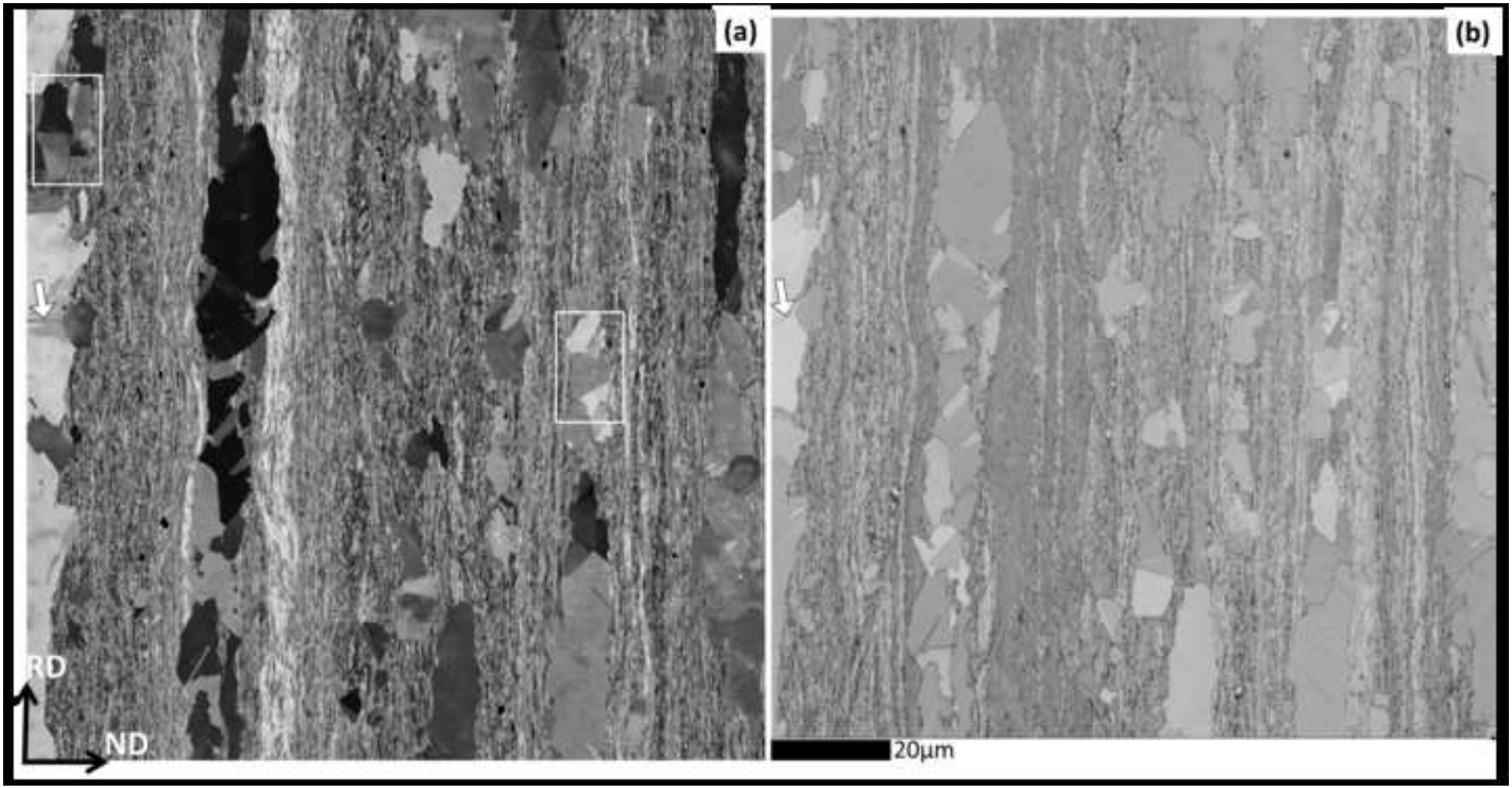

Figure2c-e

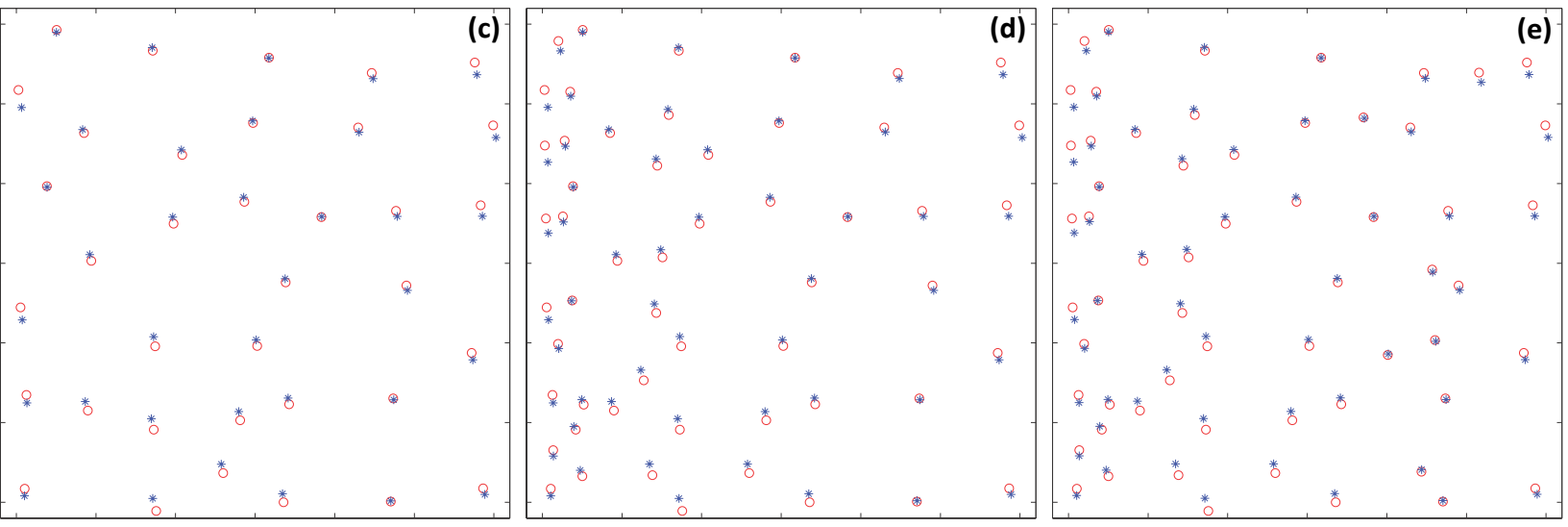

Figure3

Click here to download high resolution image

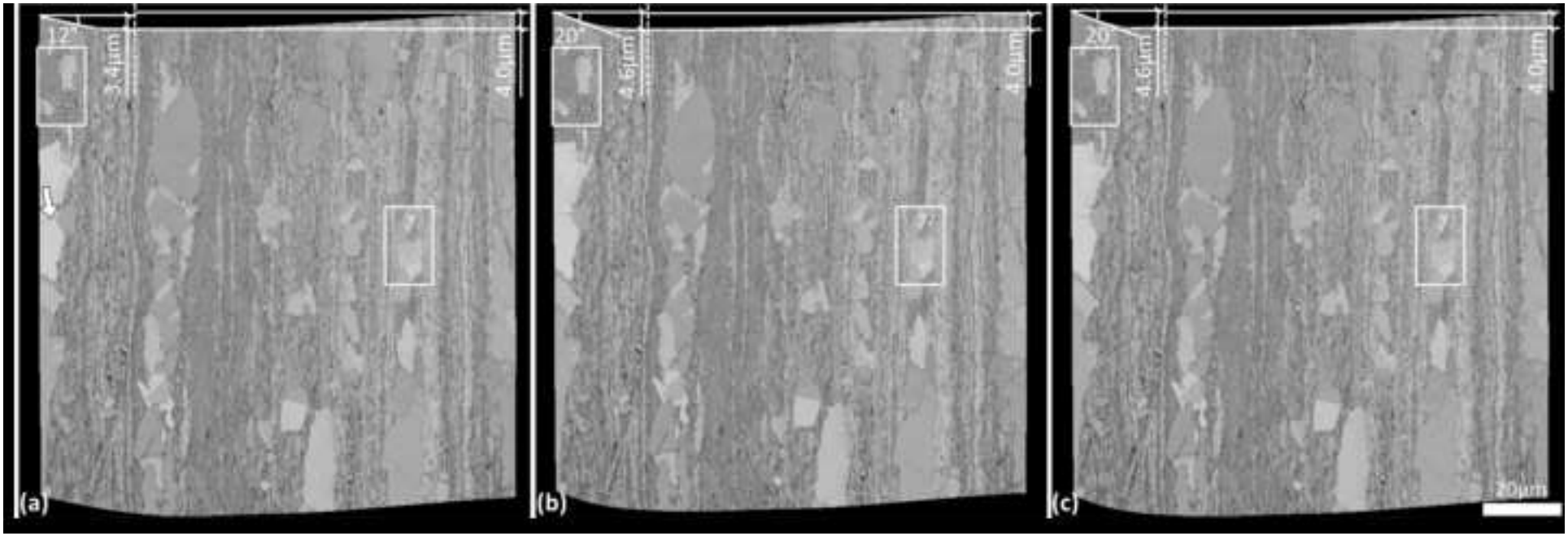

Figure4

Click here to download high resolution image

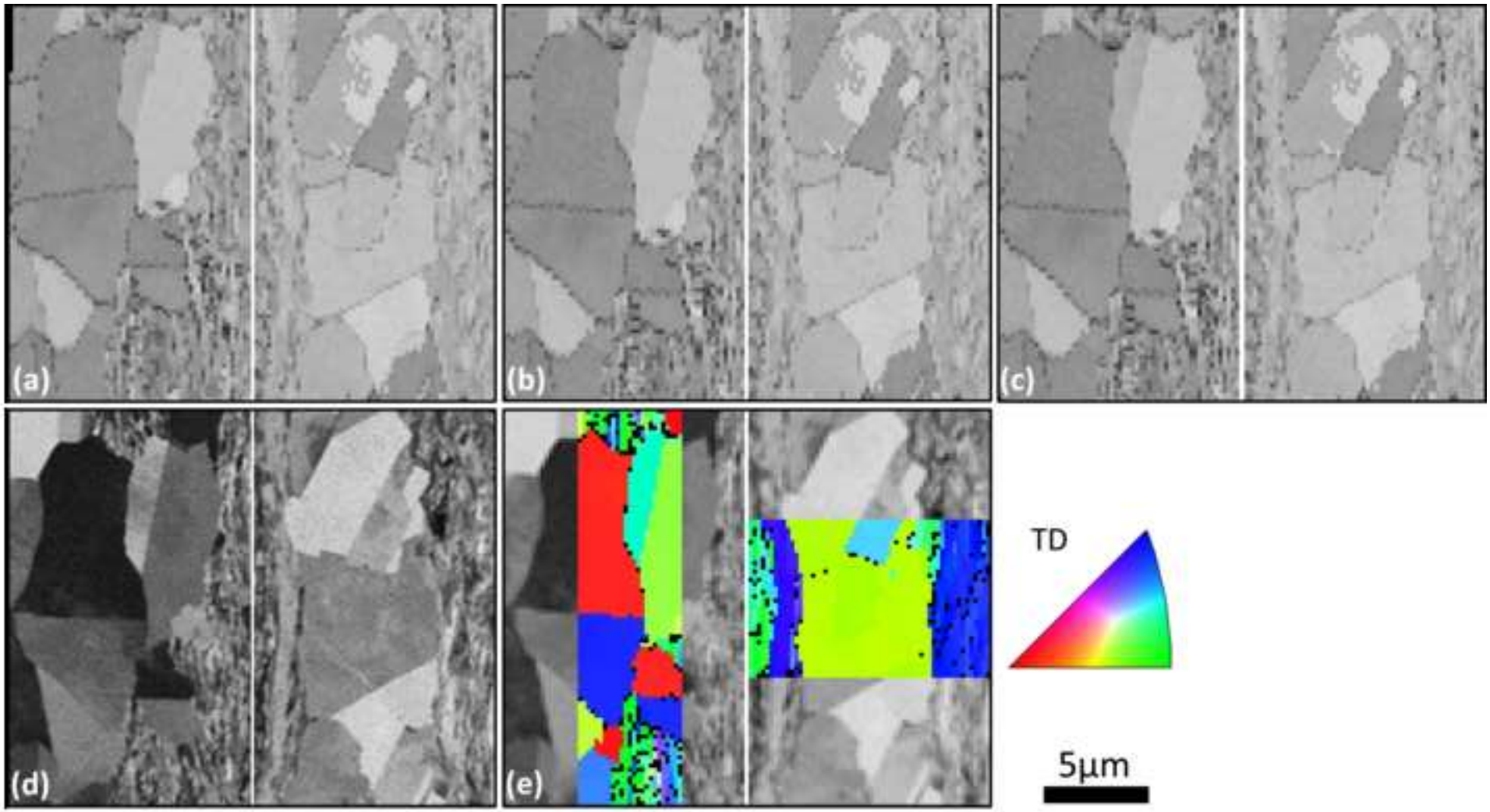

Figure5

Click here to download high resolution image

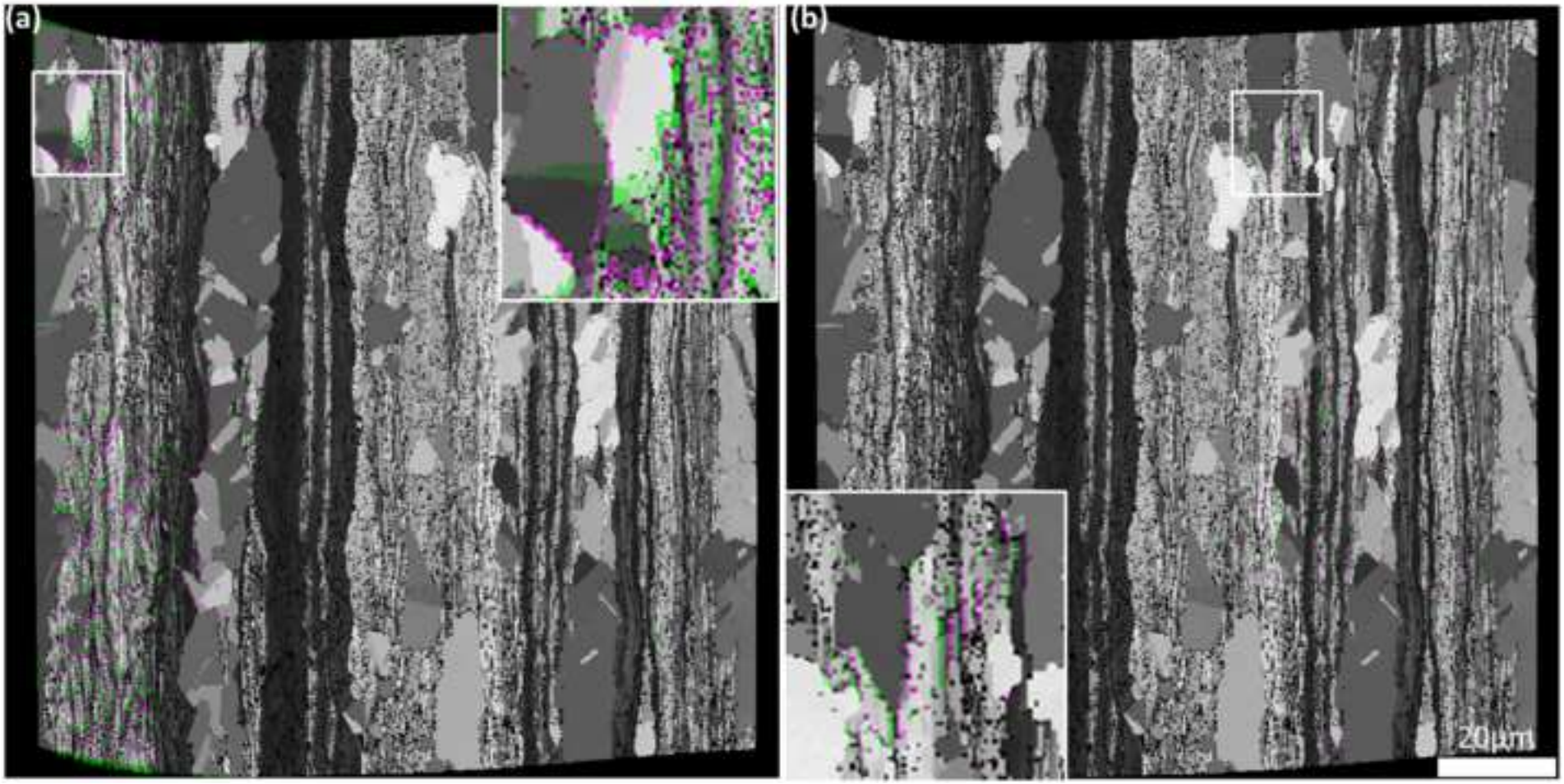

Figure6

Click here to download high resolution image